Frequency participation by using virtual inertia in wind turbines including energy storage

Xiao, Zhao xia; Huang, Yu; Guerrero, Josep M.; Fang, Hongwei

Published in:
Proceedings of 43rd Annual Conference of the IEEE Industrial Electronics Society, IECON 2017

DOI (link to publication from Publisher):
10.1109/IECON.2017.8216419

Publication date:
2017

Document Version
Early version, also known as pre-print

Frequency Participation by Using Virtual Inertia in Wind Turbines Including Energy Storage

Xiao Zhaoxia[1], Huang Yu[1], Josep M. Guerrero[2]

1.Tianjin Key Laboratory of Advanced Technology of Electrical Engineering and Energy

Tianjin Polytechnic University, P. R. China, Email: xiaozhaoxia@tjpu.edu.cn

2. Dept. of Energy Technology, Aalborg University, Denmark, joz@et.aau.dk www.microgrids.et.aau.dk

***Abstract*—With the increase of wind generation penetration, power fluctuations and weak inertia may attempt to the power system frequency stability. In this paper, in order to solve this problem, a hierarchical control strategy is proposed for permanent magnet synchronous generator (PMSG) based wind turbine (WT) and battery unit (BU). A central controller forecasts wind speed and determines system operation states to be sent to the local controllers. These local controllers include MPPT, virtual inertia, and pitch control for the WT; and power control loops for the BU. The proposed approach achieve at the same time both output power smoothing and frequency participation. Simulation results confirm the effectiveness of the proposed control strategy in different scenarios.**

Keywords—Wind power, virtual inertia control, frequency regulation, microgrids, automatic generation control (AGC)

I. INTRODUCTION

The penetration of the wind power installed is increasing worldwide, however impacting seriously the grid performances [1]-[4]. Wind power fluctuations may result in frequency instabilities, especially in weak-grid situations. Recently, more permanent magnet synchronous generator (PMSG) based wind turbines (WT) are becoming more popular in wind farms duo to the higher performances required in new grid code. In contrast to the conventional synchronous generators, PMSG, because of the use of back-to-back converters, disturbances in the wind generator little affect the main grid. However, the WT rotor speed is decoupled from the grid frequency, which may result in a lack of inertia, i.e. frequency changes will not produce power variations, as it is desired in a power system [5]-[6].

Further, placing energy storage systems in wind power systems can effectively smooth wind power fluctuations, and can improve the output controllability of the wind power generation, which has great significance to the frequency regulation [7]-[8].Relevant research has been done on wind generation frequency regulation [9]-[10]. In order to make WTs to participate in frequency regulation, we can use power reserve and rotor inertia controllers. A method to do that consist on reserving some amount of power, so that the power generation is out from the optimal value. Another way to achieve it is to reduce the output active power by using pitch control, thus when the frequency drops, reserved power may be used to support the system frequency. However, the abovementioned methods are at the expenses of reducing wind power efficiency.

Alternatively, rotor inertia control can be also used providing a short time power support for DFIG-based WTs [9]. In [10], frequency-rotor speed coordinated control strategy is adopted to reduce sudden WT torque changes, and to adjust rotor speed when the frequency changes. However, in [11] was pointed out that rotor speed recovery may cause the secondary frequency drop down.

To solve this problem, in [12] by introducing energy storage may help wind power systems in frequency regulation. In this work, a flywheel is used in combination with a DFIG for these purposes. In [13], BU is connected to the ac bus of the stationary synchronous compensator, while in [14] a super capacitor is be connected to the dc bus of PMSG wind power generator. Although the abovementioned methods may be used to make wind power participating in frequency regulation, they present complex implementation and control.

In order to solve wind power and frequency fluctuations, this paper uses a method to calculate the expected interchanged power flow of the wind power system tie-line, according to the predicted wind speed inside a determined time period. The designed WT-BU structure connects the BU to the ac part through an inverter. A power-frequency loop is added PMSG side converter, so that the system inertia is effectively increased. When the system frequency exceeds specified range, the wind power generation system ensures the MPPT performances, while the WT-BU

active power output is rapidly changed according to the automatic generation control (AGC) instructions. A hierarchical control structure is presented to implement those functionalities. Simulation results and analysis are given showing, the performances of the proposed approach.

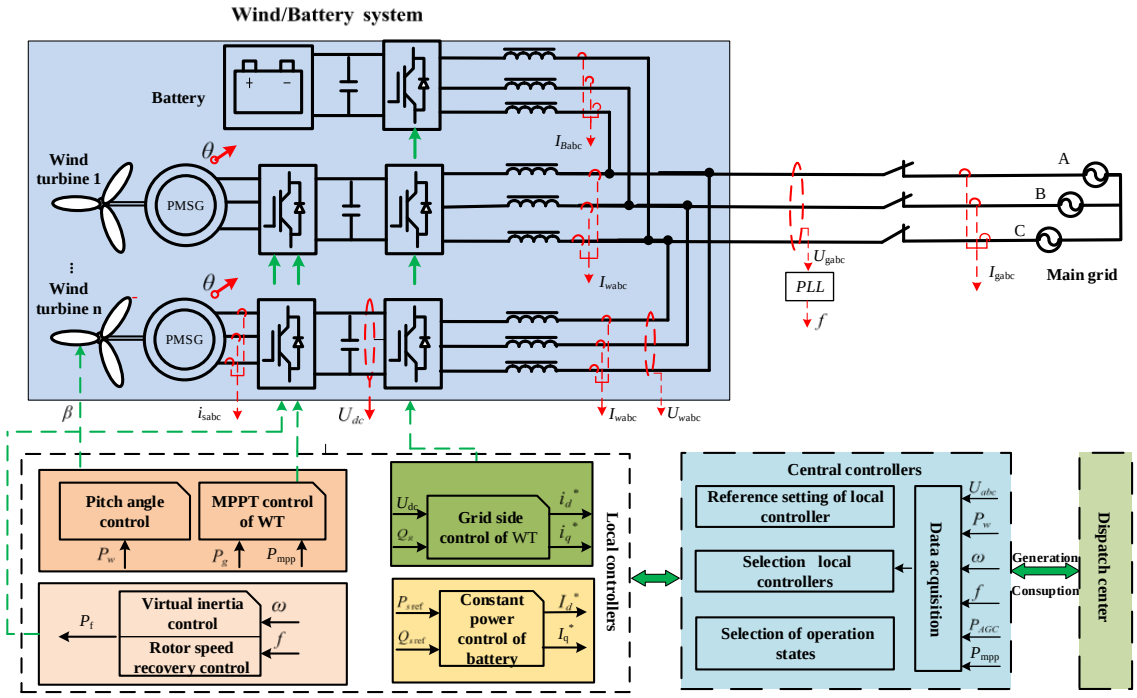

Fig. 1. Structure of WT-BU system.

II. Hybrid Structure of WT-BU System

Fig. 1 shows the hybrid WT-BU system, including the power stage and the control architecture. In this case the BU is connected to the AC side to facilitate the retrofitting. Note that adding batteries in the DC side may be more effective, but in practice it may not be suitable since it may require cooperation between WT and BU producers companies, which may not be easy in many cases. Since in our case, the hardware control between the WT and the energy storage system is completely decoupled from each other, it is more feasible in practice.

Regarding the controllers, the easiest way is to have WT-BU locally controlled and to add a central controller that can be placed in a SCADA system that may control the hybrid power system. The central controller includes wind forecasting, power calculations, system operation mode selections, battery charge/discharge management, and the real-time grid frequency detection.

Through the coordinated control of WT-BU, when the frequency of the system is nominal, the power supplies smoothed power to the main grid. Furthermore, when the frequency of the system is outside the normal range, the WT-BU power system participates in the frequency regulation.

III. Frequency Participation

A. *Kinetic Energy of the Wind Turbine*

The kinetic energy stored in the rotor blade of a WT can be expressed as:

$$E = \frac{1}{2} J\omega^2 \tag{1}$$

where J is the inertia of the wind turbine and its generator and ω is the rotor speed. When the rotor speed is ranged from ω_0 to ω_1, the difference of the kinetic energy of the wind turbine is:

$$\Delta E = \frac{1}{2} J{\omega_0}^2 - \frac{1}{2} J{\omega_1}^2 \tag{2}$$

From (2), we can conclude that the wind power system has a certain rotational kinetic energy. Conventional variable-speed WT, in order to achieve maximum wind energy capture, uses back-to-back converters in order to decouple rotor speed and grid frequency. Therefore, a frequency-dependent power command P_f can be imposed on the active power reference value of the rotor side converter controller.

Hence when the system frequency is nominal, P_f will be zero, otherwise P_f will change accordingly. This way, the kinetic energy stored in the wind power system can be converted into electrical energy in order to support the grid frequency.

B. Battery participation in power grid frequency regulation

The proposed WT-BU hybrid power system is able to follow AGC power scheduling P_{AGC} to restore the grid frequency, see Fig. 2. For instance, when the grid frequency is out from the nominal range, the WT-BU hybrid system will react according to the AGC scheduling instructions in order to quickly change its active power output thus achieving frequency restoration. The system reacts according to the following strategy to control the frequency. If the grid frequency is high, BU is charging, thus reducing the output power of the tie-line. Otherwise, if the grid frequency is low, BU is discharging, thus increasing the output power of the tie-line.

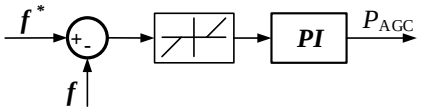

Fig. 2. Block diagram of the automatic generation control (AGC).

IV. Central Controller

The central controller takes care of the BU management and the different operation modes of the WT-BU power system.

A. Output power reference of BU inverter

The wind energy generated W_W during the scheduling period T can be expressed as follows:

$$\mathrm{W_W} = \int_0^{\mathrm{T}} \mathrm{P_W dt} \tag{3}$$

being P_W the forecast wind power generation.

Thus, during this scheduling period T, the average wind power, P_L, takes the form:

$$\mathrm{P_L} = \frac{\mathrm{W_G}}{\mathrm{T}} \tag{4}$$

If the grid frequency is nominal, the expected total active power output during the scheduling period T is the output power average over this period. At this time, the reference output power of the BU inverter can be expressed as:

$$\mathrm{P_{ref}} = \mathrm{P_L} - \mathrm{P_G} \tag{5}$$

where $\mathrm{P_G}$ is the actual output power of WT.

If the main grid requires all WTs to participate in the frequency regulation, the expected total active power output during the scheduling period T is the output power average plus the active power of frequency regulation P_{AGC} over this period. The reference output power of the BU inverter can be expressed as:

$$\mathrm{P_{ref}} = \mathrm{P_L} + \mathrm{P_{AGC}} - \mathrm{P_G} \tag{6}$$

Notice that the output power of BU, P_B, should track P_{ref}.

B. Operation modes and transition conditions

The central controller takes care of managing the different operation modes. Notice that V is the actual wind speed, while V_n is the rated nominal wind speed; f is the actual grid frequency, f_{min} and f_{max} are the minimum and maximum grid frequency. Battery maximum power charge and discharge are noted as P_{BC} and P_{BD}.

- Mode 1: If $\mathrm{V} \le V_n$, the frequency will be nominal, WT operates in the MPPT mode, and the tie-line active power of is regulated to a constant value. The reference value of the active power of the energy storage inverter is: $P_{ref} = P_{\mathrm{L}} - P_G$.
- Mode 2: If $V > V_n$, the frequency of the power grid is nominal, the pitch control of wind generation system starts working, to limit the output power of wind power the active power output of wind-energy storage system tie-line stays a constant value. The reference value of the active power of the energy storage inverter is: $P_{ref} = P_{\mathrm{L}} - P_G$.
- Mode 3: When $f > f_{max}$ and $\Delta\mathrm{P} + P_{AGC} \ge P_{BC}$ ($\Delta\mathrm{P} = P_G - P_{\mathrm{L}}$), the energy storage starts participating in the frequency regulation, $P_{ref} = P_{\mathrm{L}} - P_G + P_{AGC}$.
- Mode 4: When $f < f_{min}$ and $\Delta\mathrm{P} + P_{AGC} < P_{BD}$ ($\Delta\mathrm{P} = P_G - P_{\mathrm{L}}$), and at this time rotor speed of wind turbine $\omega \le 0.8\omega^*$, ω^* is rated speed of wind turbine, the energy storage start to adjust the frequency, $P_{ref} = P_{\mathrm{L}} - P_G + P_{AGC}$.
- Mode 5: When $f < f_{min}$ and $\Delta\mathrm{P} + P_{AGC} < P_{Bmax}$, and at the same time rotor speed of wind turbine $\omega > 0.8\omega^*$, virtual inertia starts operating. When rotor speed dropped to $0.7\omega^*$, the frequency is not restored to the nominal value, and at the same time BU starts participating in the frequency regulation $P_{ref} = P_{\mathrm{L}} - P_G + P_{AGC}$.

It should be noted that when the frequency of the power grid is too high or too low, the P_{AGC} is greater than the BU charge/discharge maximum output power, and the hybrid WT-BU system is disconnected from the power grid, running in islanded mode. Tables I present the operation modes and transition conditions of the WT-BU system.

TABLE I. Operation modes and transition conditions

Mode	*State transition condition*
1	$V \leqslant V_n$
	$f_{min} \leqslant f \leqslant f_{max}$

2	$V> V_n$ && $P_G>P_L$
	$f_{min} \leqslant f \leqslant f_{max}$
3	$f> f_{max}$ && $\Delta P+P_{AGC} \geqslant P_{BC}$
	$(\Delta P=P_G-P_L)$
4	$f< f_{min}$, $\omega \leqslant 0.8\ \omega^*$
	$\Delta P+P_{AGC} \leqslant P_{BD}$
5	$f< f_{min}$, $\omega>0.8\omega^*$
	$\Delta P+P_{AGC} \leqslant P_{BD}$ $(\Delta P=P_G-P_L)$

V. LOCAL CONTROLLER

In this Section, the local controllers of both WT and BU are presented.

A. Wind generation controller

The PMSG based WT use a back-to-back PWM converter, which avoids the use of gear box, thus improving system efficiency and reliability.

1) PMSG side control

The controller includes MPPT algorthm, pitch control, and inner current loops. In is well known that *the wind energy captured by wind turbines can be expressed as:*

$$P_w = \frac{1}{2}\rho\pi R^2 C_p v^3 \tag{7}$$

where ρ is air density, R is the radius of the wind turbine, and C_p is the wind energy utilization factor, being a function of the pitch angle β and the tip speed ratio λ, $\lambda = \omega R/v$, while ω is the speed of wind turbine. When the pitch angle is constant, the WT runs at the optimum tip speed ratio, so that it can get the maximum wind energy utilization factor C_{pmax}. Therefore, at a certain wind speed, the WT maximum power is only related to the rotor speed:

$$P_{opt} = k\omega^3 \tag{8}$$

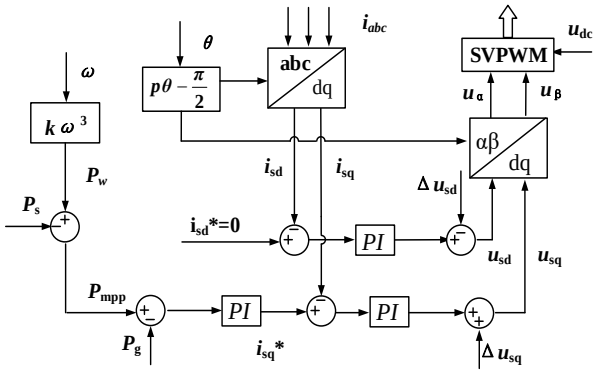

Fig. 3. Block diagram of generator side control

$$k=\frac{1}{2}\rho\pi R^5 C_p \frac{\omega^3}{\lambda^3} \tag{9}$$

The PMSG rotor-side control block diagram is shown in Fig. 3. The generator side converter is designed to achieve maximum power tracking for wind energy by using stator flux linkage vector control. By using the synchronous reference frame transformation in *dq* axis, the stator voltage equation can be expressed as:

$$\begin{cases} u_{sd} = -R_s i_{sd} - L_s \frac{di_{sd}}{dt} - \omega_e L_s i_{sq} \\ u_{sq} = -R_s i_{sq} - L_s \frac{di_{sq}}{dt} - \omega_e L_s i_{sd} + \omega_e \varphi \end{cases} \tag{10}$$

The electromagnetic torque can be obtained as:

$$T_e = \frac{3}{2} p\left[\varphi i_{sq} + \left(L_{sd} - L_{sq}\right) i_{sq} i_{sd}\right] \tag{11}$$

where R_s is the stator resistance, L_{sd} and L_{sq} is the stator inductance, i_{sd} and i_{sq} is the stator current, u_{sd} and u_{sq} is the stator voltage, ω_e is synchronous angular velocity, φ is permanent magnet flux linkage and p is the number of pole pairs. Considering that the current d-axis component is always fixed to 0, then the electromagnetic torque can be expressed as

$$T_e = \frac{3}{2} p\varphi i_{sq} \tag{12}$$

2) Grid Side Control

The aim of the grid side controller is to stabilize DC bus voltage and to achieve *P/Q* decoupling control. Grid side controller block diagram is shown in Fig. 4.

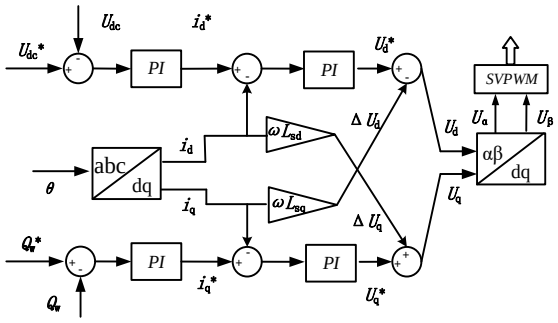

Fig. 4. Wind power grid side controller

The grid-side converter *dq* model can be expressed as:

$$\begin{cases} u_{gd} = -R_g i_{gd} - L_g \frac{di_{gd}}{dt} + \omega_g L_g i_{gq} + e_{gd} \\ u_{gq} = -R_g i_{gd} - L_q \frac{di_{gq}}{dt} - \omega_g L_g i_{gd} \end{cases} \tag{13}$$

where e_{gd} and e_{gq} is the grid voltage, i_{gd} and i_{gq} is the grid voltage, R_g and L_g is the resistance and inductance of grid-side converter, and ω_g is grid angular frequency.

The grid side controller uses grid *P/Q* calculation as:

$$\begin{cases} P_g = e_{gd} i_{gd} + e_{gq} i_{gq} = e_{gd} i_{gd} \\ Q_g = e_{gd} i_{gq} - e_{gq} i_{gd} = e_{gd} i_{gq} \end{cases} \quad (14)$$

From (13), i_{gd} and i_{gq} references can be achieved by independent controlling P_g and Q_g.

3) Pitch control

When wind speed exceeds the rated wind speed, active power output of the WT needs to be limited by changing the wind turbine pitch angle β, hence reducing the wind energy capture coefficient. The output power P_w of the current generator is compared with the reference power P_w^*. The error is processed by the PI controller to produce the required β^* (see Fig. 5). Thus the pitch angle is changed accordingly, so that the WT output power is kept at reference P_w^*.

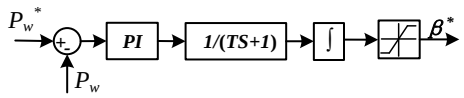

Fig. 5. Pitch control.

4) Virtual inertia and rotor speed control

Fig. 6 shows the block diagram of the virtual inertia and the rotor speed control. The virtual inertia controller detects when the grid frequency drop down, making the rotor speed decreasing, thus the rotating kinetic energy is released to prevent further decreasing the grid frequency.

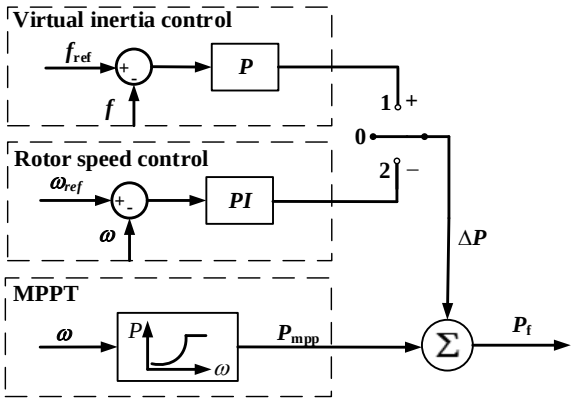

Fig. 6. Rotor inertia control and speed recovery control

When starting the virtual inertia loop, the controller will connect ΔP to switch 1 (see Fig. 6), and the power reference will change according to the frequency deviation that will go through a P controller that will added over the MPPT output (P_{MPP}). In order to prevent WT losing too much kinetic energy, when the rotor speed dropped down to 0.7 times of the rated value, the virtual inertia loop is disconnected, and ΔP will be connected to switch 0. If the grid frequency is nominal, the speed recovery control will start, connecting ΔP to switch 2. Then, the rotor speed control will generate the power reference, which will be obtained by using the rotor speed deviation through a PI controller that will be subtracted from P_{MPPT}.

B. BU Inverter Power Control

The BU inverter power controller structure is shown in Fig. 7. The grid voltage u_{abc} and inverter grid current i_{abc} are used to calculate *P*/*Q*, controlling those to follow P_{ref}/Q_{ref}, and then control I_d/I_q through internal current loops.

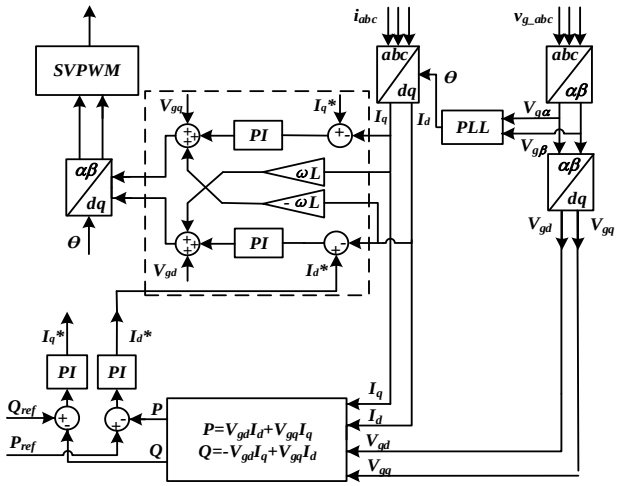

Fig. 7. Energy storage inverter power control

VI. MICROGRID CASE STUDY

The model of a hybrid WT-BU system connected through a tie-line to a microgrid system was developed by using Matlab/Simulink. The selection and switching of the operating modes of the WT-BU system embedded in the central controller is realized based on the *stateflow* toolbox. The main parameters of the system are shown in Table II. The rated capacity of the microgrid is 10MW, and the unit regulation power of the wind storage system is 1MW/Hz. The nominal grid frequency is f_n=50 Hz, with +/-1% of error, so that the maximum and minimum frequencies where f_{max}=50.5 Hz and f_{min}=49.5 Hz. The microgrid control includes a secondary control based on AGC to restore the frequency.

Wind speed curve, as shown in Fig. 8, cut the wind speed at 6m/s, and the rated wind speed is 12m/s. According to the above mentioned, according to the wind speed curve, the calculation of the tie-line power is P_L =940kW.

TABLE II SIMULATION PARAMETERS

Wind turbine parameters	Value
Wind turbine radius /m	27.5

Rated wind speed m/s	12
Air density kg/m^3	1.225
Rated power /MW	1.1
Best tip speed ratio	6.325
Wind energy maximum utilization factor	0.4385
Pitch control proportional coefficient	0.01

Permanent magnet wind turbine parameters	Value
Rated power /kW	1.1
Flux linkage	4.74
Inertia /Joules	411258
Pole pairs	42
Stator resistance /Ω	0.006
d-axis inductance /mH	1.704
d-axis inductance /mH	1.216
Grid side converter parameters	**Value**
Line inductance /mH	0.2
DC side capacitance /μF	60000
DC side voltage /V	1200
Inner loop regulator gain k_{p1}, k_{i1}	1, 10
Outer loop regulator gain k_{p2}, k_{i2}	2, 120
Rotor side converter parameters	**Value**
Rotor side d-axis current inner loop k_{p3}, k_{i3}	25, 1
Rotor side q-axis current inner loop k_{p4}, k_{i4}	40, 9
Active power outer loop k_{p5}, k_{i5}	0.0032, 0.059
Rotor inertial control loop k_{p6}, k_{i6}	250000, 0
Speed recovery loop k_{p7}, k_{i7}	350000, 200000
Energy storage system parameters	**Value**
Rated voltage of battery /V	1
Battery capacity /Ah	800
Battery maximum charge current	0.2C
Battery maximum discharge current	0.4C
Maximum discharge power P_{BD}	600 kW
Maximum charge power P_{BC}	-160 kW
PQ controls d-axis current inner loop k_{p8}, k_{i8}	2, 20
PQ controls q-axis current inner loop k_{p9}, k_{i9}	2, 20
PQ control active power outer loop k_{p10}, k_{i10}	0.001, 0.5
PQ control reactive power outer loop k_{p11}, k_{i11}	0.001, 0.5

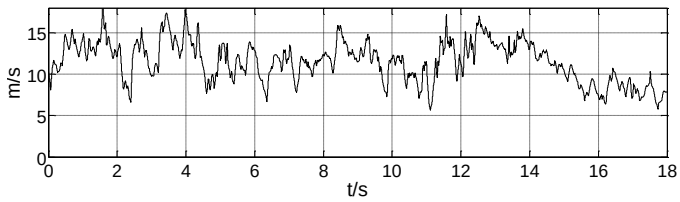

Fig. 8. Wind speed curve

The simulation results of the wind storage system in different operating modes are shown in Fig 9. F and f are frequency of the wind-energy storage system before and after the participation in the frequency regulation in Fig. 9 (a). Fig. 9 (b) is the wind generation output power; Figure 9 (c) is the generator rotor speed; Figure 9 (d) is DC voltage of wind power. Figure 9 (e) shows battery charging and discharging current. Figure 9 (f) is battery output power; Figure 9 (g) shows the active power output of WT-storage system.

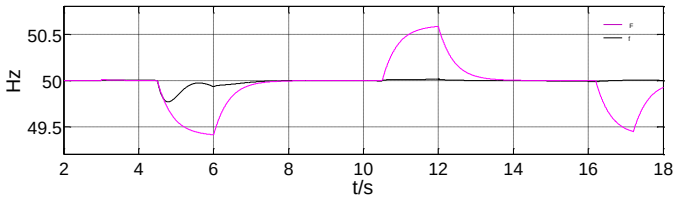

(a) Frequency participation of the WT-storage system

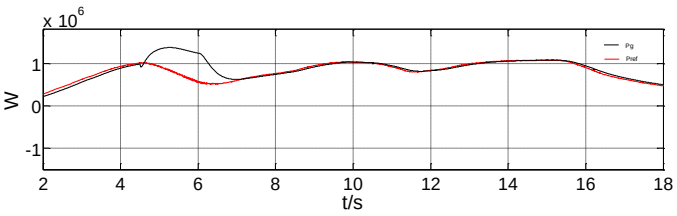

(b) Output power of wind turbine

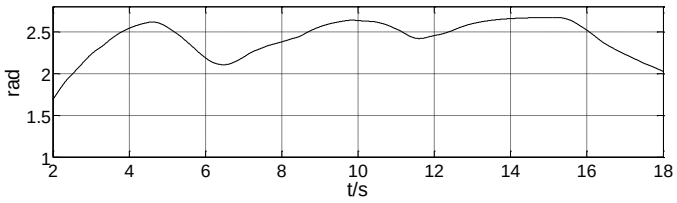

(c)Rotor speed

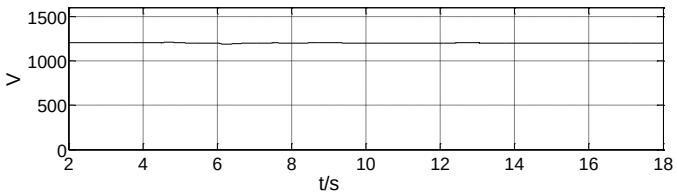

(d) DC voltage of wind power

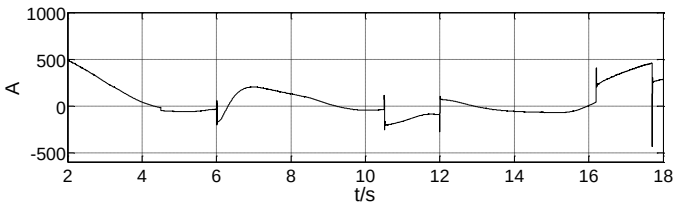

(e) Battery charging and discharging current

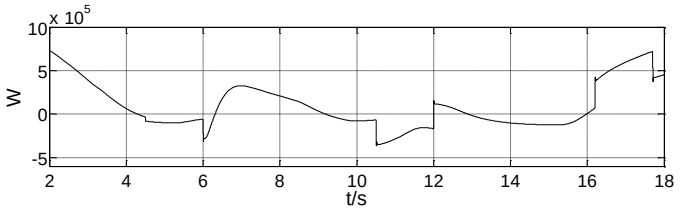

(f) Battery output power

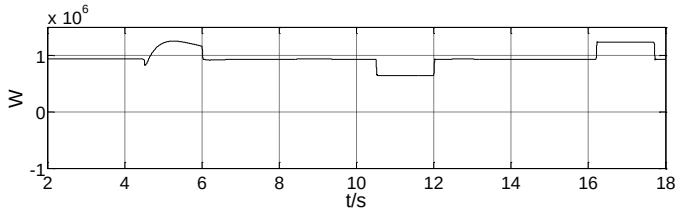

(g) Active power output of WT-storage system

Fig. 9. Simulation results.

VII. CONCLUSION

This paper proposed a grid-connected wind generation system retrofitted with a battery energy storage unit. The proposal includes inertia emulation by linking the rotor speed with the frequency, taking into account speed constraints and coordinating the actions between WT and BU.

The paper introduces a control architecture in order to achieve a good integration of the WT-BU system with the power system, thus achieving the following salient features:

- Output power smoothing
- AGC power schedule following
- Frequency regulation and participation

Simulation results shown the hybrid WT-BU power system with the proposed control architecture operates properly in the context of a small weak grid.

ACKNOWLEDGEMENT

This work was supported by the Tianjin Science and Technology Support Program Key Project and National Natural Science Foundation of China (15JCZDJC32100, 17JCZDJC31300 and 51577124).

REFERENCES

[1] Miao Fufeng, Tang Xisheng, Qi Zhiping, “Capacity optimization of energy storage participating to wind plant primary frequency regulation,” Advanced Technology of Electrical Engineering and Energy, 2016，(04):23-29.

[2] Lou Suhua, Yang Tianmeng, Wu Yanwu. Coordinated optimal operation of hybrid energy storage in power system accommodated high penetration of wind power. Automation of Electric Power Systems, 2016,(07):30-35.

[3] J. W. Choi, S. Y. Heo and M. K. Kim, "Hybrid operation strategy of wind energy storage system for power grid frequency regulation," in IET Generation, Transmission & Distribution, vol. 10, no. 3, pp. 736-749.

[4] Miao Fufeng, Tang Xisheng, Qi Zhiping, “Analysis of frequency characteristics of power system based on wind farm-energy storage combined frequency regulation,” High Voltage Engineering, 2015，(07)：2209-2216.

[5] Wang Haijiao, Jiang Quanyuan, “An overview of control and configuration of energy storage system used for wind power fluctuation mitigation,” Automation of Electric Power Systems, 2014,(19):126-135.

[6] Tang Xisheng, Miao Fufeng, Tang Xisheng, “Survey on frequency control of wind power,” Proceedings of The Chinese Society for Electrical Engineering, 2014,(25):4304-4314.

[7] Wang Haijiao, “Analysis of frequency characteristics of power system based on wind farm-energy storage combined frequency regulation,” Advanced Technology of Electrical Engineering and Energy, 2012(14): 152-155.

[8] Miao Fufeng, Tang Xisheng, Qi Zhiping. Analysis of frequency characteristics of power system based on wind farm-energy storage combined frequency regulation.Advanced Technology of Electrical Engineering and Energy, 2012(14): 152-155.

[9] Jiang Ping, Xiong chuanhua. A control scheme design for smoothing wind power fluctuation with hybrid energy storage system. Automation of Electric Power Systems, 2013,(01):122-127.

[10] R. Xiang, X. Wang and J. Tan, "Operation control of flywheel energy storage system with wind farm," Proceedings of the 30th Chinese Control Conference, Yantai, 2011, pp. 6208-6212.

[11] N.Y.Abed, S. Teleke and J. J.Castaneda, "Planning and operation of dynamic energy storage for improved integration of wind energy," 2011 IEEE Power and Energy Society General Meeting, San Diego, CA, 2011, pp. 1-7.

[12] S. M. Muyeen, H. M. Hasanien and J. Tamura, "Reduction of frequency fluctuation for wind farm connected power systems by an adaptive artificial neural network controlled energy capacitor system," in IET Renewable Power Generation, vol. 6, no. 4, pp. 226-235, July 2012.